Geopersia ***10*** *(2), 2020, PP. 405-418* *DOI: 10.22059/GEOPE.2020.296150.648525*

Characterization of the Bazman geothermal field, the southeast of Iran

Farkhondeh Askari Malekabad[1], Reza Jahanshahi*[1] Rahim Bagheri[2]
[1] *Department of Geology, Faculty of Science, University of Sistan and Baluchestan, Zahedan, Iran, Post Code: 9816745639, P.O. Box: 98135-674, Tel: +989131790969, Fax: +98543446565*
[2] *Faculty of Earth Sciences, Shahrood University of Technology, Shahrood. Iran, Tel. Fax: 02332396007, Post Code: 3619995161*
**Corresponding author, e–mail: jahanshahireza@science.usb.ac.ir*
(*received: 18/01/2020 ; accepted: 15/04/2020*)

Abstract
The Bazman volcano in the southeast of Iran is considered to be a dormant volcano. To study the hydrogeochemistry and geothermometry, sixteen water samples were collected from the thermal and cold springs. Temperature of the cold springs range from 28.1 to 36.6 °C while mean temperature of the thermal spring waters is ~42 °C. Generally, the salinity values of the water samples vary from 1102 in the cold spring to 10250 µS/cm in the thermal springs. The water samples are categorized into three types: Cl –Na, Cl–HCO3–Na–and SO4–Na. The composition values of δ^2H and $\delta^{18}O$ in the thermal springs were resulted from water–rock interaction or underground evaporation in the deep depths. Since the thermal springs have a different temperatures but similar chloride content, it seems that a conductive cooling mechanism is occurring in the geothermal system. Based on the geothermometry results, the equilibrium temperature of the deep reservoir estimated from ~120 to 145 °C. The fraction of the cold water mixed with the warm water ascending is estimated to be ~0.94. Finally, the depth of thermal water circulation is estimated to ranging from 1.9 to 3 km under two different scenarios.

Keywords: *Geothermometry, Stable Isotopes, Geothermal Field, Water–rock Interaction, Bazman Volcano*

Introduction

Hydrochemical analysis and geothermometry can serve as a tool to estimate the equilibrium temperature of geothermal reservoirs (Blasco *et al.,* 2018). The equilibrium temperature establishes a necessary information for geothermal energy development plants before deep–well drilling (Huang *et al.,* 2018). In a geothermal zone, the deep circulation of groundwater generally can change the local thermal gradients and heat distribution (Allen *et al.*, 2014). Thermal springs as natural discharges from the underground thermal reservoirs are a surface sign of the presence of these kind resources in the area of interest (Karimi *et al.,* 2017). Characterization of the physicochemical and stable isotopic content in the water of the thermal springs have been used by many previous researchers to determine the origin of waters and temperature of the thermal reservoirs (Navarro *et al.*, 2004; Chenaker *et al.,* 2018; Mohammadi *et al.,* 2010; Parisi *et al.*, 2011; Furi *et al.*, 2012; Afsin, 2014; Sharifi *et al.*, 2016; Cinti *et al.,* 2017; Foued *et al.,* 2017, Karimi *et al.*, 2017; Blasco *et al.,* 2018; Ferguson *et al.,* 2018, Huang *et al.*, 2018; Morales–Arredondo *et al.*, 2018; Pang *et al.*, 2018; Chatterjee *et al.,* 2019). Some researchers used these characteristics to present a conceptual flow system (Han *et al.*, 2010; Mohammadi *et al.,* 2010; Farr & Bottrell, 2013; Alçiçek *et al.*, 2018; Rezaei *et al.*, 2018 and 2019) and evaluating processes of water–rock interaction (Dotsik *et al.,* 2006; Han *et al.,* 2010; Asta *et al.*, 2012; Farr & Bottrell, 2013).

In Iran some of researchers have focused on the hot springs in Zagros Zone (Kompani Zare & Moore, 2001; Mohammadi *et al.,* 2010), Alborz Zone (Raghimi & Yakhkeshi, 2002; Sharifi *et al.*, 2016; Karimi *et al.,* 2017; Afshar *et al.*, 2017; Rezaei *et al.*, 2019) and Central Iran Zone (Yazdi *et al.,* 2015; Mohammadi & Sahraei Parizi, 2013; Rezaei *et al.*, 2018). However, here we try to study the Bazman geothermal system in East Iranian Ranges and Makran Zone in the southeast of Iran where does not studied significantly until now. Since the Bazman volcano only occasionally smokes, it is a dormant volcano (Bahadori *et al.,* 2019, Naderi *et al.,* 2020). There are fourteen cold and two thermal water springs discharging the Bazman volcano area. In the study area due to absence of pumping wells in the area, groundwater discharge only via these few springs from local hard rock aquifer. This volcano has a potential to be developed for the geothermal power plant energy. Prior to this research, no work studied the geothermometry of the Bazman geothermal system. Therefore, this study tries to evaluate the thermal and cold water springs scattered over the Bazman volcanic area with emphasis on: (i) hydrogeochemistry of both the cold and thermal waters, (ii) origin of the water

and possible salinity source of the springs, (iii) estimating the depth of circulation and equilibrium temperatures of the geothermal reservoir, and finally (iv) mixing percentage of the cold–warm waters in the area.

Experimental

Study area

Iran's plateau is separated into nine tectono–stratigraphic zones (Berberian & King, 1981) (Fig 1a). The study area is situated in the west of the Sistan Suture zone and north of the Makran zone. There are three geomorphological features in the margin of Makran continental including (i) Makran accretionary prisms which cover the southeastern of Iran to the western of Pakistan (Fig. 1a); (ii) Jazmurian depression situated at the southern of Lut Block (Fig 1a) and (iii) a zone composed of basaltic to rhyolitic rocks forming the Makran Volcanic Arc (stratovolcanoes) and resulted from the Makran subduction (Saadat & Stern, 2011; Farhoudi & Karig, 1977). Based on Ar – K ages, in the Bazman area, basalts were erupted at 0.6 Ma and 4.6 Ma, respectively (Saadat & Stern, 2011; Conrad *et al.,* 1981). Sedimentary rocks in the area contain Jamal (Upper Permian) and Sardar (Carboniferous) formations where are composed of siltstone, shale, sandstone and limestone (Fig 1b).

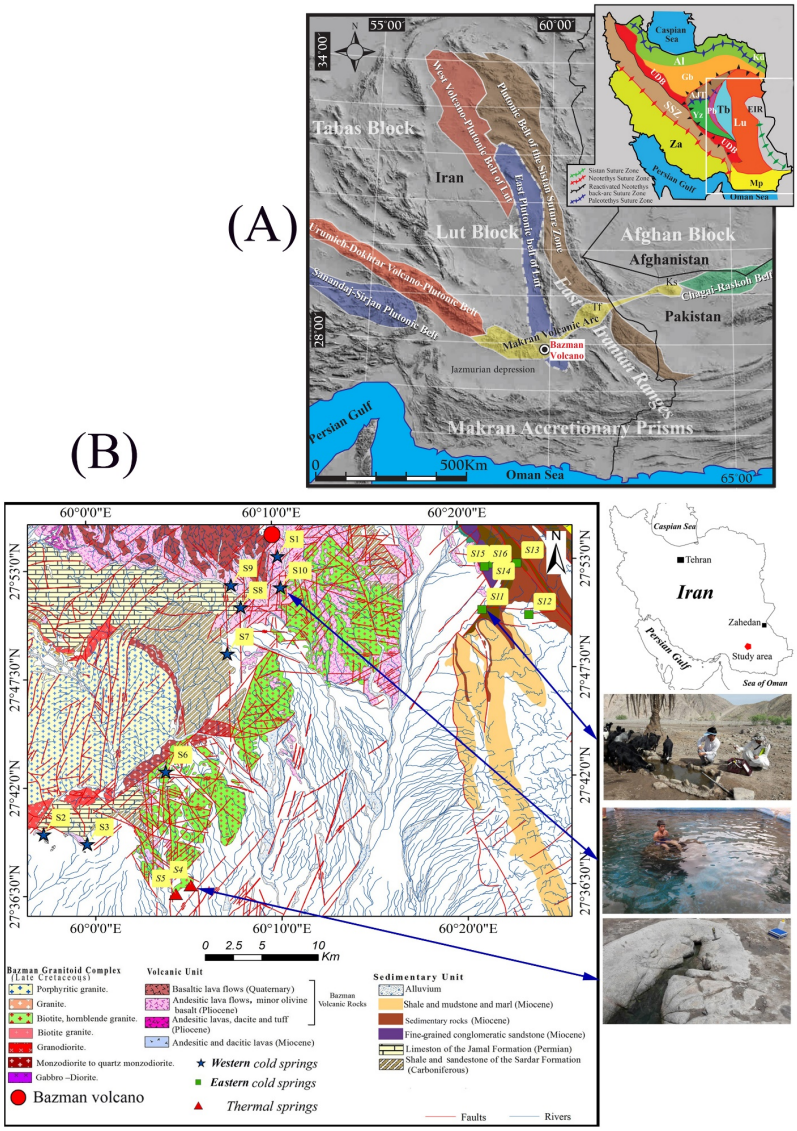

Figure 1. According to Berberian & King (1981): units of main tectono-stratigraphic in Iran (Ghodsi *et al*., 2016) (a) map of geological setting and the thermal and cold springs in the Bazman geothermal zone (b).

These rocks have been intruded by Bazman granitoids complex (Ghodsi *et al.,* 2016). Owing to erosion and the complex has a lower elevation than the surrounding sedimentary rocks. The Bazman area has arid climate characterized by mean annual rainfall of less than 120 mm. The highest, lowest and mean temperatures for the study area are +46 °C, –9 °C and 25.5 °C, respectively. There are two thermal and fourteen cold springs scattered over the area (Fig. 1b). The cold water springs can be grouped into the eastern and western springs. The eastern springs are discharging from the sedimentary rocks (e.g shale, marl, and sandstone) while the western cold springs are mostly discharged from granitoids, basalts and carbonate rocks. However, the thermal springs are situated over the granitoids complex. The largest cold spring (S10) and the thermal springs (S4 and S5) are usually used by the native people for drinking and bathing/balneotherapy purposes.

Methodology

Sampling and analysis

Groundwater samples were collected from two thermal and fourteen cold springs in June 2017 (Fig 1b) and then sent immediately to labs for chemical and stable isotopes (δ^2H and $\delta^{18}O$) measurements. During water sampling, first the waters were filtered and then poured into clean polyethylene bottles (300 mL). The pH, temperature and EC were measured *in situ* by portable instruments pH–meter (WalkLAB–TI900) and EC–meter (AQUA–TC 485). The water samples were treated with HNO_3 solution to analyze the major cation. The Mg, Ca, K, Na, Al, Br and Li ions, and SiO_2 were analyzed via IC MS system (HP Agilent 4500). The SO_4 was measured by spectrophotometry (HACH–RD2000), and HCO_3 and Cl were determined by titration methods. To evaluate the uncertainty of the measurements, ion balance equation was used and the ionic balance error for each water sample calculated to be less than 5%. Oxygen and hydrogen isotope ratios in water samples were measured by an OA–ICOS device and them represented according to VSMOW international standard. The chemical and isotopic measurements data are listed in Table 1.

Modelling and statistical methods

Mineral saturation indices of calcite, dolomite, gypsum, halite, albite, analcime, diaspre, jarosit, laumontite, brucite, forsterite, kaolinite, microcline, wollstanite, monticellite and sanidine in the water samples were calculated by the PHREEQC software (Parkhurst & Appelo, 1999) for hydrochemistry and geothermometry investigation.

Pearson's correlation coefficients between variables of hydrogeochemistry were calculated according to normalized data using SPSS software Version 17 (Table 2). In addition, to identify the multivariate relationships between pH, EC, SO4, Cl, HCO3, Na, K, Mg and Ca in water samples, principal components analysis (PCA) were also applied using SPSS software (Table 3).

Equations of the chemical geothermometers (Fournier, 1979; Rybach & Muffler, 1981; Nieva & Nieva, 1987; Kharaka & Mariner, 1989) were used to estimate the temperatures of the deep–water.

Table 1. Physicochemical properties of the thermal and cold water springs in the study area (EC in µS/cm, ions content in mg/L, and δ^2H and $\delta^{18}O$ values in ‰ VSMOW).

	Name	EC	TDS	T°C	pH	HCO3	Cl	SO4	Ca	K	Mg	Na	SiO2	Al	Li	Br	δD	$\delta^{18}O$	Error %
Cold springs	S1	1322	730.5	28.1	8.0	163.5	167.3	163.1	28.2	3.8	9.7	195.0	20.4	0.02	0.1	0.2	-4.13	-15.75	0.01
	S2	1350	868.9	34.8	7.6	281.6	184.0	150.4	65.0	4.4	27.5	156.0	8.4	0.03	0.2	0.6	-4.46	-14.6	1.95
	S3	1270	843.4	33.9	7.6	297.7	165.0	138.9	67.0	4.4	26.5	144.0	8.0	0.07	0.2	0.1	-3.99	-13.49	2.01
	S6	1541	1049.9	33.4	7.8	313.8	191.4	254.4	89.3	3.9	30.1	167.0	10.1	0.06	0.1	0.6	-4.58	-15.56	4.98
	S7	2190	1184.2	32.1	7.7	279.6	357.1	162.4	63.6	16.8	36.8	268.0	14.7	0.06	0.6	2.7	-4.85	-20.9	0.83
	S8	2140	1366.7	35.5	7.5	363.1	395.3	201.8	96.9	16.8	34.9	258.0	17.6	0.06	0.6	0.6	-4.85	-20.71	4.65
	S9	2085	1300.5	33.9	7.3	363.1	368.3	189.8	98.0	19.2	31.1	231.0	18.8	0.06	0.5	2.9	-4.65	-20.43	4.88
	S10	1102	631.3	34.2	7.3	97.1	177.2	151.6	38.1	8.5	6.9	142	28.7	0.05	0.1	0.9	-5.06	-23.72	4.67
	S11	7290	5119.1	30.8	7.1	272.1	880.8	2385.4	376.7	6.5	114.6	984	8.3	0.08	0.3	2.8	-2.77	-15.75	4.66
	S12	2290	1573.4	36.6	7.5	147.9	203.1	700.2	111.5	2.6	15.1	330	6.5	0.09	0.2	1.5	-2.35	-11.94	3.38
	S13	1818	1296.3	30.3	7.6	308.7	66.6	598.9	77.9	1.7	35.5	247	6.6	0.05	0.2	1.0	-1.14	-9.98	4.80
	S14	4320	3441.8	31.9	7.7	266.7	600.8	1601.3	220.9	4	62.2	790	8.5	0.08	0.2	5.3	-1.28	-8.98	2.87
	S15	2472	1587.4	28.3	8.9	45.6	168.4	952.3	98	2.4	8.7	420	7.2	0.09	0.1	2.7	0.04	-10.65	2.81
	S16	1222	853.1	35.4	8.3	179.8	64.9	361.8	38.2	1.5	19	188	12.7	0.05	0.1	0.8	-0.77	-8.6	2.53
	Max	7290	5119.1	36.6	8.9	363.1	880.8	2385.4	376.7	19.2	114.6	984	28.7	0.09	0.6	5.3	0.04	-8.6	-
	Min	1102	631.3	28.1	7.1	45.6	64.9	138.9	28.2	1.5	6.9	142	6.5	0.02	0.1	0.1	-5.06	-23.72	-
	Mean	2550.3	1724.8	32.7	7.7	236.8	308.4	658.5	117.1	7.3	36.2	352.8	13.2	0.06	0.3	1.8	-3.12	-15.2	-
Hot sprin	S4	10040	4797.8	43.9	8.7	75.6	2635.0	428.0	508.5	21.5	29.2	1400.0	13.1	0.11	2.1	20.0	-4.4	-24.1	2.82
	S5	10250	5276.5	40.1	8.7	62.2	2723.0	433.8	623.6	22.0	28.9	1383.0	13.6	0.09	1.9	12.8	-4.54	-23.99	4.15
	Mean	10145	5037.15	42	8.7	68.9	2679	430.9	566.05	21.75	29.05	1391.5	13.35	0.1	2	16.4	-4.47	-24.045	-

Table 2. The matrix of Pearson's correlation for hydrogeochemical properties in the water samples

	EC	pH	Cl	SO_4	HCO_3	Na	Ca	Mg	K
EC	1								
pH	0.022	1							
Cl	**0.946**	0.089	1						
SO_4	**0.605**	-0.180	0.425	1					
HCO_3	-0.157	-0.363	-0.231	0.008	1				
Na	**0.954**	-0.024	**0.949**	**0.564**	-0.135	1			
Ca	**0.827**	0.260	**0.831**	**0.508**	-0.229	**0.709**	1		
Mg	**0.667**	-0.428	**0.567**	**0.733**	0.274	**0.638**	0.497	1	
K	**0.762**	-0.201	**0.810**	0.273	0.013	**0.832**	0.476	**0.578**	1

Table 3. Component loadings of the EC, pH and major ions using method of principal component analysis

Variable	SO_4	Cl	HCO_3	Na	K	Mg	Ca	EC	pH	% of variance	Cumulative %
PC1	**0.664**	**0.945**	-0.106	**0.959**	**0.807**	**0.765**	**0.819**	**0.976**	-0.067	57	57
PC2	0.265	-0.224	**0.753**	-0.063	0.107	0.526	-0.325	-0.105	**-0.84**	20	77

Also modelling of the equilibrium state at various temperatures via PHREEQC cod (Parkhurst & Appelo, 1999) was used for identifying the temperature of deep–water. Different saturation states of the minerals in the thermal springs were obtained by keeping constant the chemical composition of thermal water samples and assuming various water temperatures (D'Amore *et al*., 1987; Lopez–Chicano, 2001; Mohammadi *et al.,* 2010).

Results and discussion

Water chemistry

The results of the chemical analysis are presented in Table 1. The pH values range from 7.1 to 8.9 (Fig 2a) which indicating a neutral to low alkaline waters. The water samples with higher pH are possible related to either carbonate minerals of the Jamal Formation or weathering of silicate minerals of the igneous rocks. Water temperature in the thermal springs ranges from 40 °C at spring S4 to 43.9 °C in the spring S5 while in the cold springs it varies from 28.1 °C in the spring S1 to 36.6 °C in the spring S12. The EC values from groundwater samples range from 1102 in the spring S10 to 10250 µS/cm in the spring S5. In fact, the cold springs have a fresh water and the thermal springs have brackish water (Fig 2b). The concentration of Cl^- in the thermal waters ranges from 2335 to 2723 mg/L while in the cold waters it varied from 64.9 – 969.8 mg/L. The Piper and Stiff diagrams (Fig. 2c) indicate that the eastern cold springs have the Na–SO_4 water type while the thermal and western cold springs are of the Na–Cl water type. The SO_4 water type can be attributed to the dissolution of gypsum of shale, marl and sandstone rocks (Sardar Formation) by the groundwater of the study area. According to the molar ratio of Na/Cl (Fig 3a), the cold water springs are mostly plotted above the line of Na/Cl = 1; most probably due to the weathering of Na–bearing silicate minerals (Eq. 1) and Na–Ca cation exchange. However, the waters of the thermal springs are plotted near the line of Na/Cl = 1 and = 0.86 may owing to the halite dissolution. Figs. 3b, c and d demonstrate that beyond the dissolution of carbonate minerals (calcite and dolomite), the origin of calcium in the water samples comes from minerals of gypsum, pyroxenes, amphibole and Ca–plagioclase.

$$2NaAlSi_3O_8+11H_2O+2CO_2 \leftrightarrow Al_2Si_2O_5(OH)_4+2Na^+ +2HCO_3^- +4H_4SiO_4 \quad (1)$$

Figs. 3e to 3h show the saturation indices calculated for calcite, dolomite, gypsum and halite of the water of the springs. All water samples are mostly supper–saturated in regards to calcite and dolomite, which indicating that these minerals tend to precipitate in the geothermal system. Otherwise, most of the water samples are under–saturated with respect to halite and gypsum; therefore, groundwater enables to significantly dissolve these minerals and affect the water quality of the study area.

Diagrams of total dissolved solid (TDS) vs. Br (Rittenhouse, 1967) and the ratio of Br/Cl versus Li/Cl (Bagheri *et al*., 2014) in Fig 4 were used to identify the water salinity sources in the study area. As shown in Fig 4a, the water samples are located around Group IV suggesting that the salinity of the springs may attribute to the effect of dissolution of salt minerals on water quality in the area. However,

the thermal springs tends to fall in Group I as a past seawater. Also, Fig 4b shows that the cold spring waters are plotted in the range of evaporite to freshwater formations, while the thermal springs are attributed to the halite dissolution.

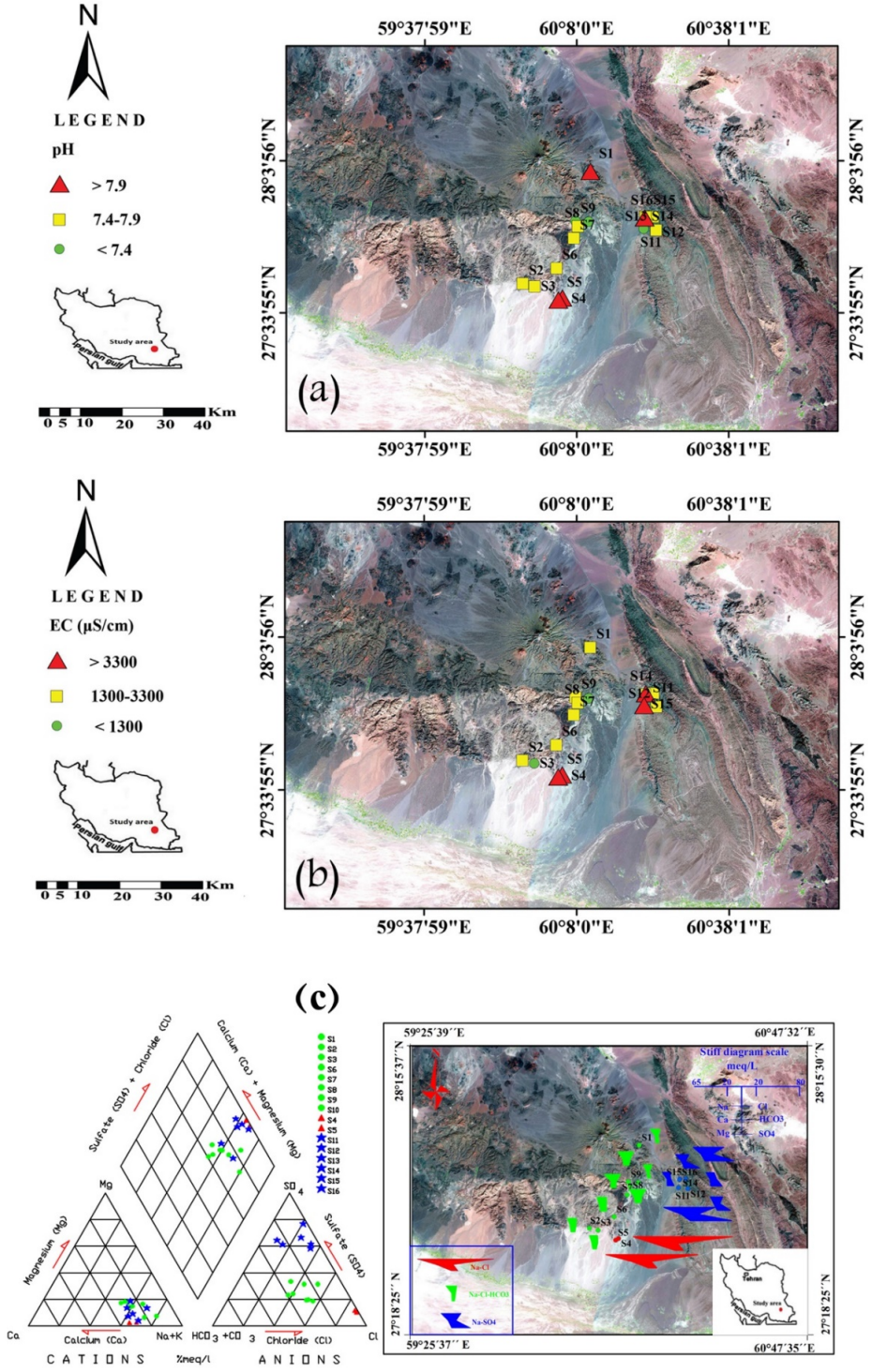

Figure 2. Spatial distribution map of pH (a), EC (b), Piper and Stiff diagrams (c) of the cold and thermal water springs in the study area

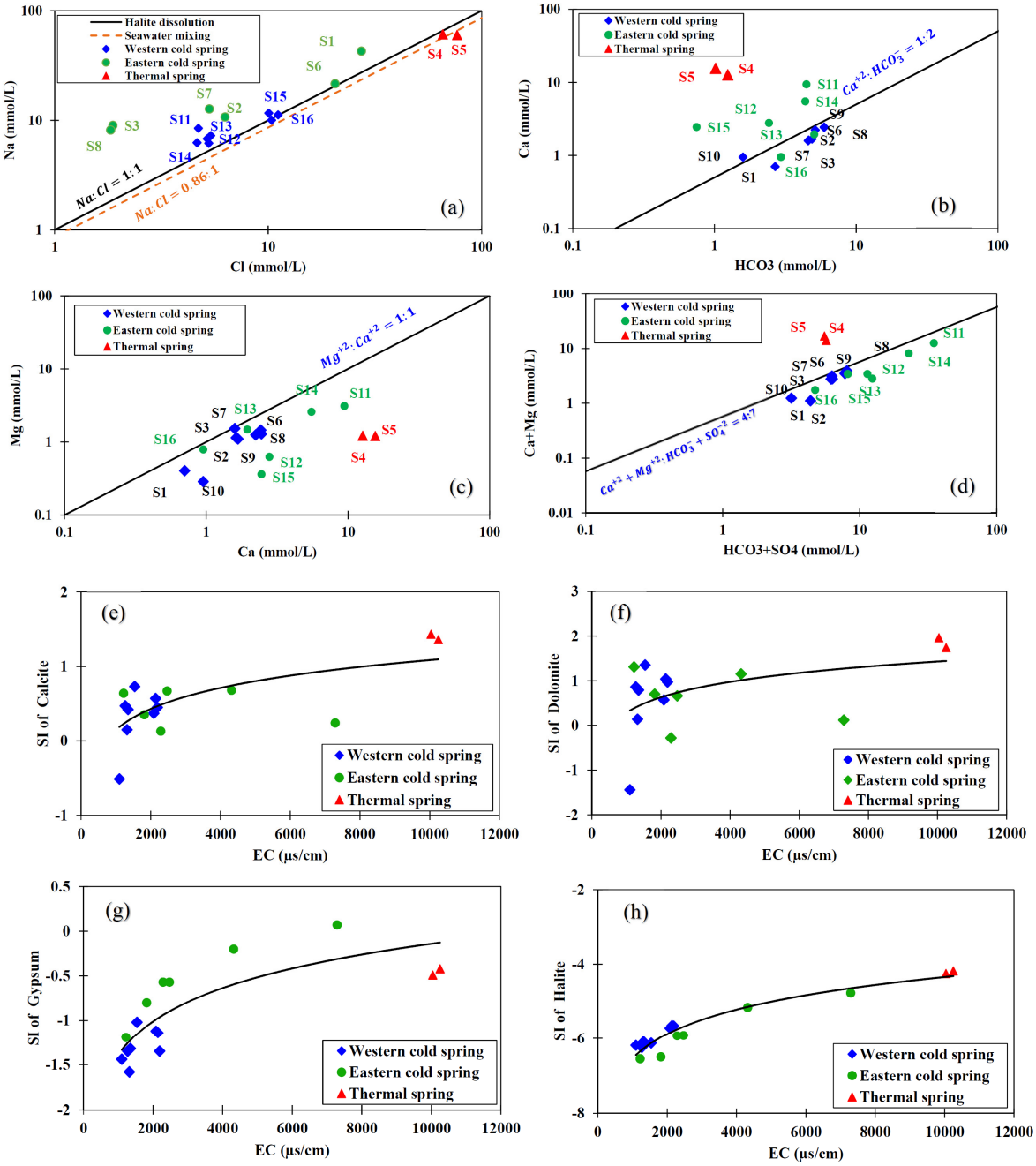

Figure 3. The molar ratio of Na/Cl (a), HCO3/Ca (b), SO4/Ca (c) and (SO4+HCO3)/(Ca+Mg) (d) the saturation indices of calcite (e), dolomite (f), gypsum (g) halite (h) in the cold and thermal water springs in the study area.

Statistical methods

Theoretically, as the water circulation depths for the cold and thermal springs are generally different than each other, it is expected that the chemistry of the cold and thermal waters is dissimilar in the study area. Given this, statistical methods should be applied separately for the cold and thermal springs to obtain better results. Nevertheless, here we consider both them together since there is only two thermal. Table 2 shows that the EC values have a high correlation with all the ions except for HCO_3. The HCO_3 has mostly a negative correlation with other ions. The correlations between pH and other parameters are mostly week and negative and it shows a buffering reactions. The weak acid anions generated by dissolved CO_2 are the most common.

When it dissolved in water, CO_2 combines with water as H_2CO_3. Then this weak acid via a series of reactions creating a buffer system:

$$CO_{2(g)} + H_2O = H_2CO_3 \rightarrow H^+ + HCO_3^- \rightarrow H^+ + C0_3^{2-} \quad (2)$$

The factor analysis performed on physicochemical parameters (EC, pH, and major ions) indicate that there are two main factors controlling the physicochemical characteristics in the area where they cumulatively clarify 77% of the total variance (Table 3). The first principal component (PC1) clarifies 57% of the total variance which it has high loadings on Cl, K, Na, Ca and EC and a moderate loading on SO_4 and Mg, indicating the significant role of mineral weathering on the groundwater chemistry in the study area. The second principal component (PC2) contributes 20% of the overall variance, which has positive loadings on HCO_3 and negative loadings on pH. It may owing to buffering reactions. According to hierarchical cluster analysis (HCA), the springs are grouped into four clusters (Fig 5) where the cold samples are mostly in cluster 4 and the thermal springs fall in a different group than the cold water springs.

Hydrogen and oxygen stable isotopes

In the cold and thermal springs of the study area, the δ^2H and $\delta^{18}O$ values range from – 24.1 to – 8.6‰ and – 5.06 to 0.04‰, respectively. The isotopic results were compared to the local meteoric water line (LMWL) for the Sirjan region (to the west of the area), as the nearest available LMWL to the area (δ^2H= 7.12 $\delta^{18}O$ +15.92 presented by Jahanshahi & Zare, 2017). The isotopic compositions of the water of the springs are plotted in Fig. 6a where the western cold springs plotted roughly on the LWML while the eastern cold springs show a higher enrichment in δ^2H and $\delta^{18}O$. The thermal springs are fell near the western cold spring but with a little bit lower δ^2H. Since the study area has an arid climate, it seems that the rainfall before percolating to groundwater has been affected by evapotranspiration and this is resulted in the isotope enrichment in the eastern cold spring's water.

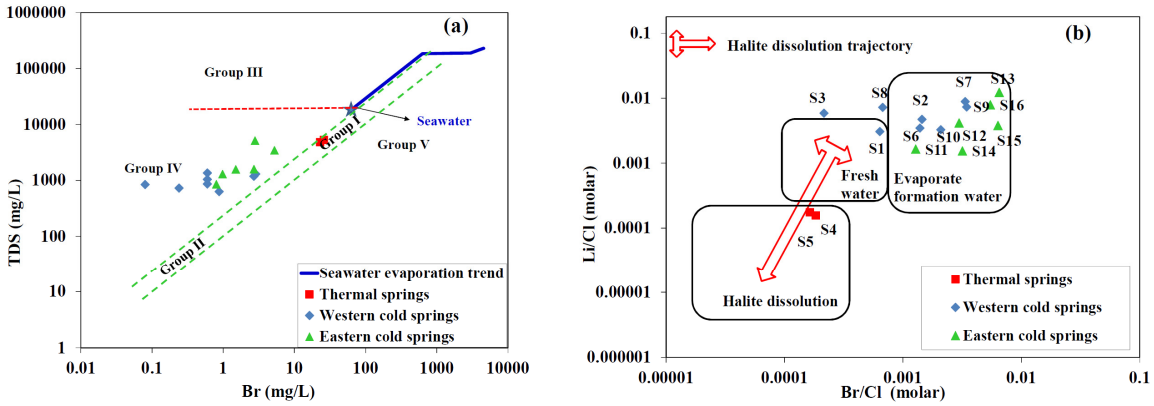

Figure 4. The relationships between TDS and Br (after Rittenhouse, 1967) (a) and, Li/Cl and Br/Cl (after Bagheri *et al*., 2014) (b).

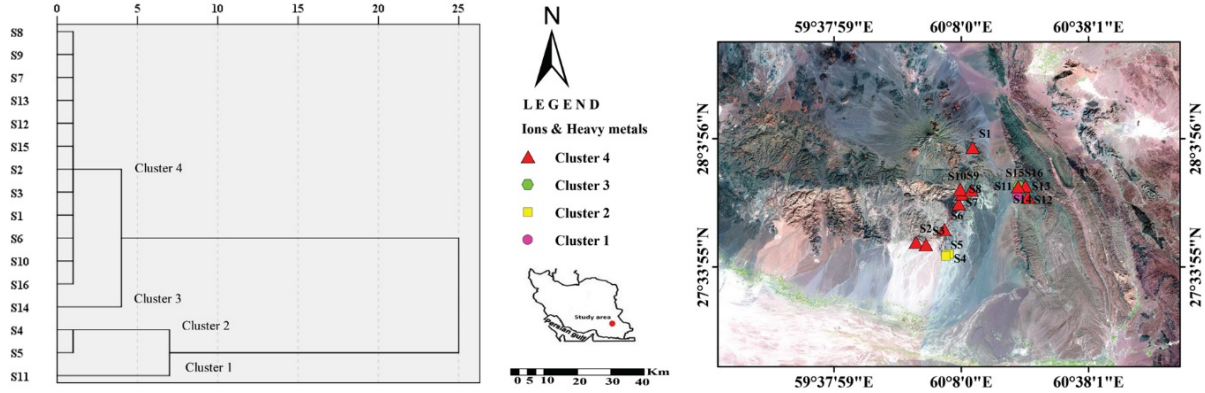

Figure 5. Dendrogram of the hierarchical and spatial distribution map of the cluster analysis.

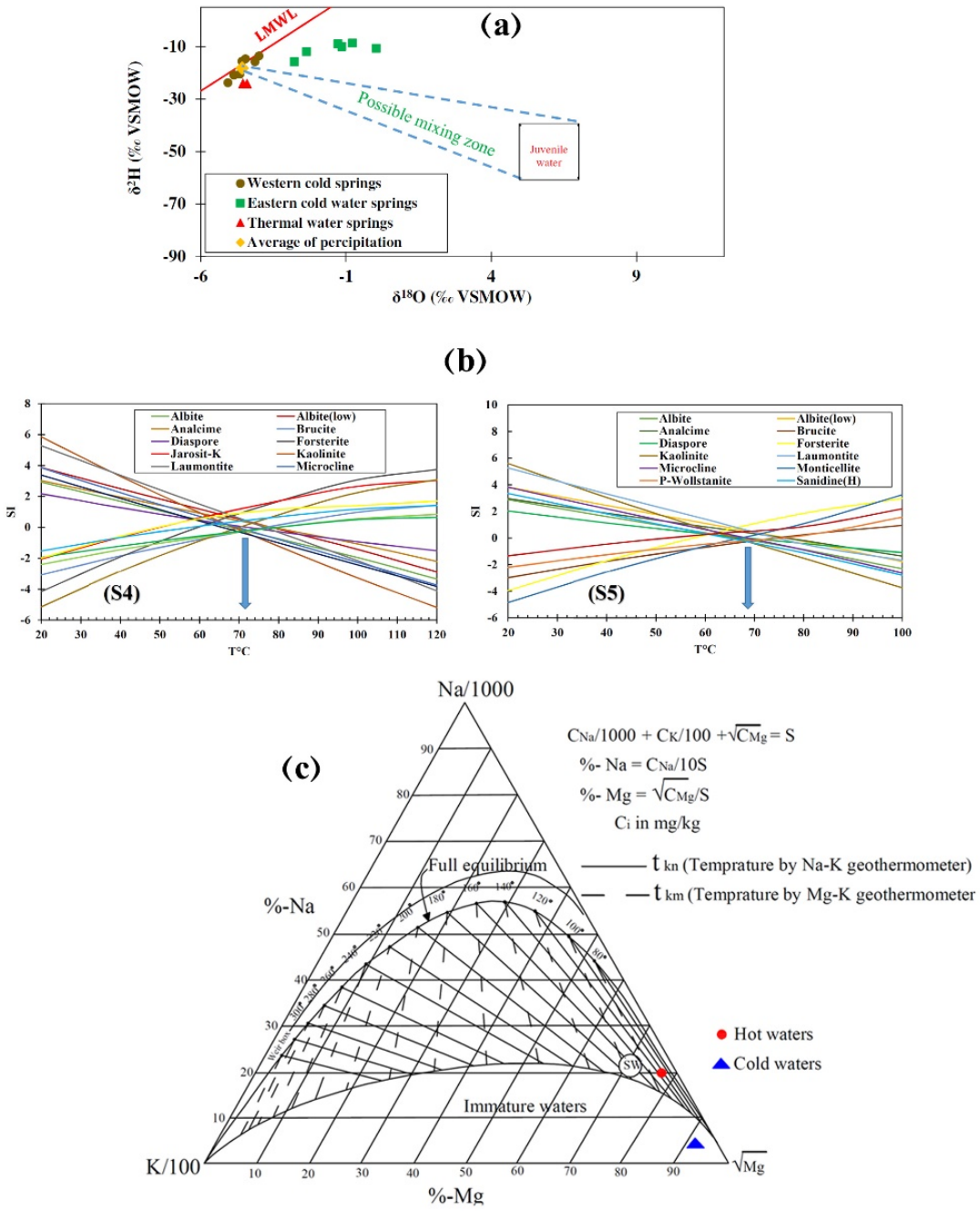

Figure 6. The stable isotopic composition (δ18O and δ2H) in the water of the springs, LMWL (Jahanshahi & Zare, 2017) and the mixing zone between juvenile water and average of precipitation (a) Diagrams of the mineral equilibrium of thermal springs S4 and S5 (b), Na–K–Mg triangular diagram (after Giggenbach, 1988) for the water samples (c) in the study area.

Moreover, Fig. 6a can also be used to explore the effect of juvenile water on the $\delta^{18}O$ and $\delta^{2}H$ content in thermal waters. According to Hoefs (2008) juvenile water has never been part of the surficial hydrologic cycle and it originates from the degassing of the earth's mantle. According to the isotopic composition values for juvenile water ($\delta^{2}H = -60 \pm 20‰$ and $\delta^{18}O = +6 \pm 1‰$) that suggested by Ohmoto (1986), Fig. 6a indicates that the isotopic contents of the hot springs are not located in the mixing zone amidst the average of isotopic composition of precipitation and juvenile water. Therefore, one can conclude that the thermal waters do not affected by the juvenile water significantly.

Otherwise, isotope enrichment observed in the thermal springs can be resulted from water–rock interaction and underground evaporation in the deep depths. Ascending hot water generates steam in a depth where pressure decreases rapidly and it named as 'underground boiling or evaporation'. This phenomenon causes the depletion and enrichment of the isotopic composition of $\delta^{18}O$ and $\delta^{2}H$ in the steam and water respectively (Bahadori *et al.,* 2019).

Geothermometry

There as various geothermometers defined by previous researchers (e.g., Fournier, 1979; Rybach & Muffler, 1981; Nieva & Nieva, 1987; Kharaka & Mariner, 1989; D'Amore *et al*., 1987) to determine the equilibrium temperature of the geothermal reservoir. In some cases, the geothermometry calculations may not be obtained correctly since hydrogeological condition may not coincide with the basic calibration and assumptions of these geothermometers (Lopez–Chicano *et al.,* 2001). The equilibrium temperature obtained for the Bazman geothermal area using the thermal water samples from S4 and S5 via geothermometers of Na–Ca–K, Na/K, Na–K–Ca with Mg correction, Na–K–Ca–Mg (Cation Composition Geothermometer (CCG)) (Nieva & Nieva, 1987), Chalcedony, Quartz–max. steam loss, Quartz no–steam loss and the modelling of the equilibrium state are listed in Table 4.

The results show that the equiliberium temperature estimated from the different geothermometers are not equal. This may be due to either the cold waters mixed with deep thermal waters and/or chemical kinetics reactions in the geothermal reservoir (Mohammadi *et al.,* 2010). The temperatures obtained from Na/K geothermometer are even less than in the temperature of the water discharging from S4 and hence are incorrect. Moreover, the temperatures calculated from the Chalcedony geothermometer are close to the temperatures of the thermal spring's water. As a result, these two geothermometers are not appropriate for the Bazman geothermal reservoir. The average of temperatures calculated by quartz geothermometers range from about 81 to 82 °C. Since Mg content in the thermal waters of the area is almost high, it seems that the temperatures calculated by Na–K–Ca geothermometer are not reliable. To address this issue, the CCG method (Nieva & Nieva, 1987) was applied to calculate the equilibrium temperature. According to this geothermometer, the temperature is calculated to vary from 138 °C to 139°C. These temperatures are significantly larger compared to those obtained from Quartz geothermometers. However, these values may be related to the deeper portions of the reservoir. Moreover, from modelling of the equilibrium state at temperatures of 72 °C to 68 °C the saturation indices of minerals were in equilibrium in the deep–water (Fig 6b) and this range of the temperatures were closed to the estimated temperature by quartz geothermometers. This may be due to mixing with cold groundwater.

Furthermore, The Na–K–Mg triangular and the Na–K–Ca–Mg diagrams (Giggenbach, 1988) were used to evaluate the chemical equilibrium of the thermal springs and their suitability to estimate the temperature of deep–water. Based on Fig 6c, the cold waters are immature waters and the thermal water samples are plotted far from the line of full equilibrium; may due to (1) high Mg content, (2) water–rock interactions, and (3) the dilution resulted from the cold water mixing. As shown in Fig. 6c, the apparent temperature of the water–rock equilibrium is ~120 °C that is closed to the temperature estimated using the CCG method in the above. According to Fournier *et al*. (1976), by assuming that S4 and S5 (as non–boiling springs) are not mixed with cold waters or the geochemical equilibration is happened after mixing, it can be considered that no steam escaped from the deep thermal waters during ascending. Given the above assumptions, the parent geothermal fluid is plotted directly above S4 and S5 in Fig 7a according to obtained temperature via CCG method and steam enthalpy tables. Also according to the boiling trend line, parent geothermal fluid can generate a boiling spring with higher Cl content than about 10000 mg/L (Fig 7a).

Table 4. Temperatures of the thermal springs and deepwater (°C) calculated by chemical geothermometers

Sample	Water temperature (T°C)	Na/K	Na-K-Ca (β= 4/3)	CCG (Nieva & Nieva 1987)	Chalcedony	Quartz-max. steam loss	Quartz no-steam loss	Modelling of the equilibrium state
S4	43.9	36	104	138	45	77	81	72
S5	40.1	48	103	139	46	78	82	68

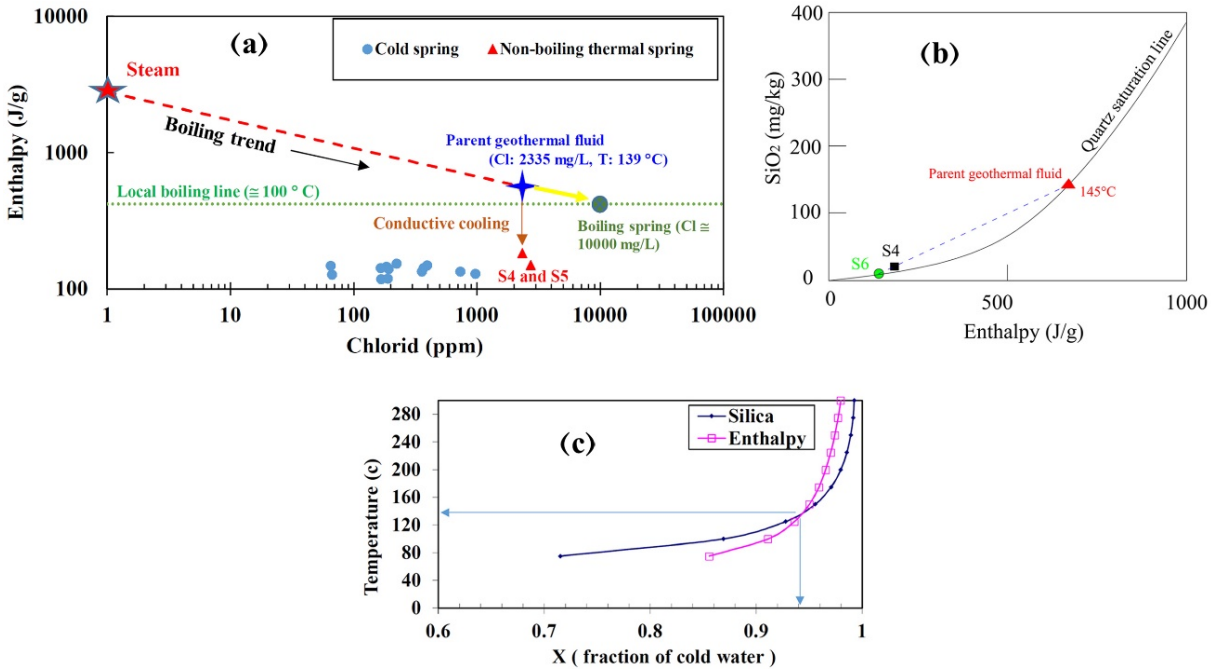

Figure 7. According to Truesdell & Fournier (1977) a hypothetical plot of chloride vs enthalpy for the cold and thermal springs (a), graph of the dissolved silica vs enthalpy to determine temperature of the parent geothermal fluid (after Truesdell & Fournier (1977)) (b) the relationship between the temperature and mixing fraction of the cold water in the thermal springs (c) in the study area.

However, by assuming that the non–boiling springs (springs S4 and S5) are not equilibrated chemically after mixing, the silica content and enthalpy of the coldest water spring (S6) and thermal spring (S4) can be plotted as Fig 7b (Truesdell & Fournier, 1977). A straight line from springs S6 to S4 is plotted in Fig 7b to intersect the quartz saturation curve. One determines the equilibrium temperature of the geothermal reservoir from the intersect point. Here the equilibrium is obtained to ~145 °C.

However, the ascending deep thermal water is probably mixed with the shallow cold groundwater. To obtain the mixture percentage, we used to the following equations (Gupta & Roy, 2007):

$$EN_C X + EN_h(1 - X) = EN_S \quad (3)$$

$$Si_C X + Si_h(1 - X) = Si_S \quad (4)$$

where EN_C, EN_h and EN_S are enthalpies of the cold, hot and the thermal spring water, respectively. The fractions of the cold water and the hot deep–water are X and (1–X), respectively. Equation (4) relates the silica content of the cold (Si_C), hot (Si_h), and the thermal spring (Si_S) water, respectively. The graphical approach presented by (Fournier and Truesdell 1973) was used to solve these equations for determining the equilibrium temperature of the reservoir and the cold water mixing fraction for the thermal springs (Fig 7c). From the figure, it is obtained that the cold water mixing fraction for the thermal spring S4 is 0.94 and of the mean equilibrium temperature of the Bazman geothermal system is ~140 °C. Furthermore, the depth of groundwater circulation is calculated as follows:

$$D = (T - T_0)/G \quad (5)$$

where D, T, T_0 and G are the depth of circulation (m); equilibrium temperature of the reservoir (°C); temperature of the thermal spring water (°C) and the geothermal gradient (°C/m), respectively. Unfortunately, there is no deep well drilled in the area to measure the local geothermal gradient; we therefore considered two different scenarios using: (1) the natural geothermal gradient of 3°C per 100 m, and (2) the normal gradient may not be reasonable because the presence of volcano in each area demonstrates the presence of a gradient higher than natural; Therefore, the maximum possible gradient for geothermal area located over the intraplate continental crust 4.6 °C per 100 m that presented by Sutherland *et al.* (2017). According to temperature of 42 °C in thermal spring S4, and average of the estimated temperatures in deep–water (132 °C), the depth of thermal waters circulation was estimated to range from 1.9 km to 3 km.

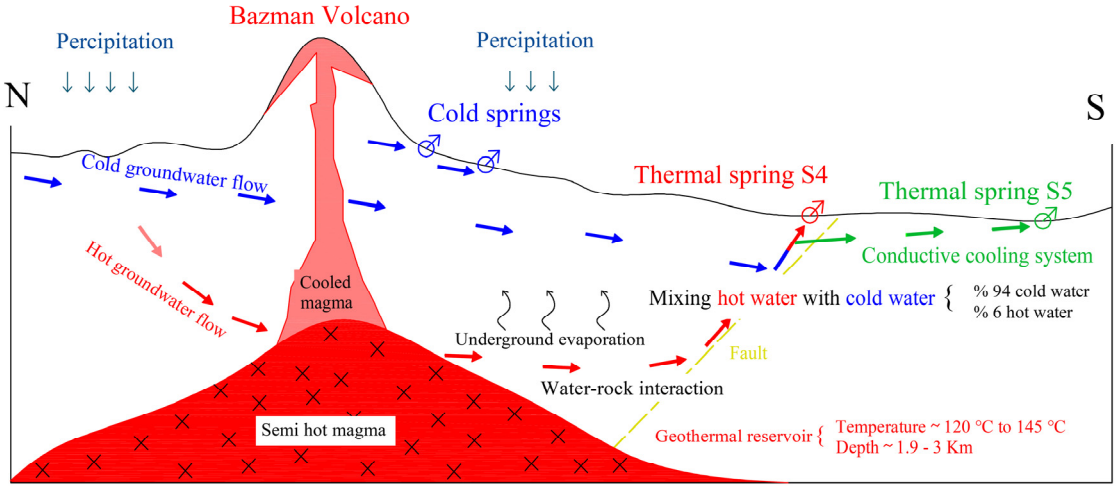

Figure 8. Simplified conceptual model for the Bazman geothermal area.

Conclusion

This study indicated that the spring's waters in the Bazman volcanic area have Cl –Na, Cl–HCO3–Na– and SO4–Na types where the dissolution of evaporite and carbonate minerals of the Sardar and Jamal formations was the main source of water salinity in the study area. The results also revealed that the evaporation of the rainfall either before or during percolating caused to the δ^2H and $\delta^{18}O$ enrichment the eastern cold–water springs. The isotopic composition of the thermal springs didn't show a significant enrichment. It was also found that the stable isotope ratios in the thermal waters did not fell in the mixing zone between juvenile water and average of precipitation, indicating no significant influence of magma on the geothermal waters. The equilibrium temperatures obtained from geothermometry ranged from 45 °C to 145 °C. Due to the presence of high Mg content in the groundwater of the study area, estimated temperatures via geothermometers of Na/K, Na–K–Ca and Chalcedony was not reliable. Since estimated temperatures of the thermal reservoirs were below 190 – 210°C, a little silicate in the deep–water tended to precipitate during movement to the ground surface, while Ca, Mg, Na and K may change due to water–rock interactions. Hence, the silicate geothermometers gave higher and reliable results. Also, the results of Na–K–Mg triangular diagram, CCG and enthalpy–silica methods were acceptable. A conceptual model for Bazman geothermal system schematically depicted in Fig. 8. According to geothermometers, temperature of the deep–water was ranged from 120 °C to 145 °C. Despite the springs were situated in a small region, temperatures of the waters had high discrepancy and this suggested mixing between the ascending thermal water and the shallow cold groundwater. The presence of the thermal springs (S4 and S5) with different temperatures and similar chloride content suggested a conductive cooling system in Bazman volcano area. If this system was an adiabatic cooling system, parent geothermal fluid could generate a boiling spring with Cl content about 10000 mg/L. Finally, mixing percentage of the cold water in the thermal springs was about 94% and the circulation depth of the deep–water was estimated in the range of 1.9 to 3 km. However, it should clearly understand that without any drilling geothermal wells, it is very speculative to estimate the depth of thermal water circulation.

References

Afshar, A., Norouzi, G.H., Moradzadeh, A., Riahi M.A., Porkhial, S., 2017. Curie point depth, geothermal gradient and heat–flow estimation and geothermal anomaly exploration from integrated analysis of aeromagnetic and gravity data on the Sabalan area, NW Iran. Pure Appl Geophys, 174: 1133–1152.

Afsin, M., Allen, D.M., Kirste, D., Durukan, U.G., Gurel, A., Oruc, O., 2014. Mixing processes in hydrothermal spring systems and implications for interpreting geochemical data: a case study in the Cappadocia region of Turkey. Hydrogeology Journal, 22: 7–23.

Alçiçek, H., Bülbül, A., Brogi, A., Liotta, D., Ruggieri, G., Capezzuoli, E., Meccheri, M., Yavuzer, İ., Alçiçek, M.C.,

2018. Origin, evolution and geothermometry of thermal waters in the Gölemezli Geothermal Field, Denizli Basin (SW Turkey). Journal of Volcanology and Geothermal Research, 349: 1–30.

Allen, D.M., Bayer, P., Ferguson, G., Blum, P., 2014. Preface: Hydrogeology of shallow thermal systems. Hydrogeology Journal, 22: 1–6.

Asta, M.P., Gimeno, M.J., Auqué, L.F., Gómez, J., Acero, P., Lapuente, P., 2012. Hydrochemistry and geothermometrical modeling of low–temperature Panticosa geothermal system (Spain). Journal of Volcanology and Geothermal Research, 235: 236:84–95.

Bagheri, R., Nadri, A., Raeisi, E., Eggenkamp, H.G.M., Kazemi, G.A., Montaseri, A., 2014. Hydrochemical and isotopic (δ18O, δ2H, 87Sr/86Sr, δ37Cl and δ81Br) evidence for the origin of saline formation water in a gas reservoir. Chem Geol, 384: 62–75.

Bahadori, D., Jahanshahi, R., Dehghani, V., Mali, S., 2019. Variations of stable oxygen and hydrogen isotope ratios in the cold and thermal springs of the Bazman volcanic area (in the southeast of Iran). Environmental Earth Sciences, 78: 663.

Berberian, M., King, G.C.P., 1981. Towards a paleogeography and tectonic evolution of Iran. Earth Sci, 18(2): 210–265.

Blasco, M., Gimeno, M.J., Auqué, L.F. 2018. Low temperature geothermal systems in carbonate–evaporitic rocks: Mineral equilibria assumptions and geothermometrical calculations. Insights from the Arnedillo thermal waters (Spain). Science of the Total Environment, 615: 526–539.

Chatterjee, S., Sinha, U.K., Biswal, B.P., Jaryal, A., Patbhaje, S., Dash, A., 2019. Multicomponent versus classical geothermometry: Applicability of both geothermometers in a medium–enthalpy geothermal system in India. Aquatic Geochemistry, doi:10.1007/s10498–019–09355–w.

Chenaker, H., Houha, B., Vincent, V., 2018. Hydrogeochemistry and geothermometry of thermal water from north–eastern Algeria. Geothermics, 75: 137–145.

Cinti, D., Tassi, F., Procesi, M., Brusca, L., Cabassi, J., Capecchiacci, F., Delgado, H. A., Galli, G., Grassa, F., Vaselli, O., Voltattorni, N., 2017. Geochemistry of hydrothermal fluids from the eastern sector of the Sabatini Volcanic District (central Italy). Applied Geochemistry, 84: 187–201.

Conrad, G., Montignary, R., Thuizat, R., Westphal, M., 1981. Tertiary and Quaternary geodynamics of southern Lut (Iran) as deduced from palaeomagnetic, isotopic and structural data. Tectonophysics, 75(3–4): 11–17.

D'Amore, F., Fancelli, R., Caboi, R., 1987. Observations on the application of chemical geothermometers to some hydrothermal systems in Sardinia. Geothermics, 16(3): 271–282.

Dotsik, E., Leontiadis, I., Poutoukis, D., Cioni, R., Raco, B., 2006. Fluid geochemistry of the Chios geothermal area, Chios Island, Greece. Journal of Volcanology and Geothermal Research, 154(3–4): 237–250.

Farhoudi, G., Karig, D.E., 1977. Makran of Iran and Pakistan as an active arc system. Geology, 5: 664–668.

Farr, G., Bottrell, S.H., 2013. The hydrogeology and hydrochemistry of the thermal waters at Taffs Well, South Wales, UK. Cave and Karst Science, 40(1): 5–12.

Ferguson, A.P.G., Fowler, C., Cantwell, C.A., Zierenberg, R.A., McClain, J., Spycher, N., Dobson, P., 2018. A conceptual geochemical model of the geothermal system at Surprise Valley, CA. Journal of Volcanology and Geothermal Research, 353: 132–148.

Foued, B., Hénia, D., Lazhar, B., Nabil, M., Nabil, C., 2017. Hydrogeochemistry and geothermometry of thermal springs from the Guelma region, Algeria. Journal of the Geological Society of India, 90(2): 226–232.

Fournier, R.O., 1979. A revised equation for the Na/K geothermometer. Geotherm Resou Council Trans, 3: 221–224.

Fournier, R.O., Sorey, M.L., Mariner, R.H., Truesdell, A.H., 1976. Geochemical prediction of aquifer temperatures in the geothermal system at Long Valley, California. U.S. Geol. Surv. Open–file Rep, 35: 76–469.

Fournier, R.O., Truesdell, A.H., 1973. An empirical Na–K–Ca geothermometer for natural waters. Geochim Cosmochim Acta, 37(5): 1255–1275.

Furi, W., Razack, M., Abiye, T.A., Kebede, S., Legesse, D., 2012. Hydrochemical characterization of complex volcanic aquifers in a continental rifted zone: The Middle Awash basin, Ethiopia. Hydrogeology Journal, 20: 385–400.

Ghodsi, M.R., Boomeri, M., Bagheri, S., Ishiyama, D., Corfu, F., 2016. Geochemistry, zircon U–Pb age, and tectonic constraints on the Bazman granitoid complex, southeast Iran. Turkish Journal of Earth Sciences, 25(4): 311–340.

Giggenbach, W.F., 1988. Geothermal solute equilibria. Derivation of Na–K–Mg–Ca geoindicators. Geochim Cosmochim Acta, 52(12): 2749–2765.

Gupta, H., Roy, S., 2007. Geothermal Energy: An Alternative Resource for the 21st Century. Elsevier, Amsterdam, the Netherlands, 292 pp.

Han, D.M., Liang, X., Jin, M.G., Currell, M.J., Song, X.F., Liu, C.M., 2010. Evaluation of groundwater hydrochemical characteristics and mixing behavior in the Daying and Qicun geothermal systems, Xinzhou Basin. Journal of Volcanology and Geothermal Research, 189(1–2): 92–104.

Hoefs, J., 2008. Stable Isotope Geochemistry, seventh edition. Springer, Berlin, 286 pp.

Huang, Y.H., Liu, H.L., Song, S.R., Chen, H.F., 2018. An ideal geothermometer in slate formation: A case from the

Chingshui geothermal field, Taiwan. Geothermics 74, 319–326.
Jahanshahi, R., Zare, M., 2017. Delineating the origin of groundwater in the Golgohar mine area of Iran using stable isotopes of 2H and 18O and hydrochemistry. Mine Water Environmental, 36(4): 550–563.
Karimi, H., Moore, F., 2008. The source and heating mechanism for the Ahram, Mirahmad and Garu thermal springs, Zagros Mountains, Iran. Geothermics, 37(1): 84–100.
Karimi, S., Mohammadi, Z., Samani, N., 2017. Geothermometry and circulation depth of groundwater in Semnan thermal springs, Northern Iran. Environ Earth Sciences, 76: 659.
Kharaka, Y.K., Mariner, R.H., 1989. Chemical geothermometers and their application to formation waters from sedimentary basins. In: Naeser ND, McCulloh TH (Eds), Thermal History of Sedimentary Basins. Springer–Verlag, New York, NY, USA, pp. 99–117.
Kompani Zare, M., Moore, F., 2001. Chemical thermometry and origin of the Dalaki mineral springs, Bushehr Province, Iran. Journal of Hydrology, (NZ) 40(2): 189–204.
Lopez–Chicano, M., Bouamama, M., Vallejeos, A., Publido, B.A., 2001. Factors which determine the hydrogeochemical behaviour of karstic springs. A case study from the Betic Cordilleras, Spain. Applied Geochemistry, 16(9–10): 1179–1192.
Mohammadi, Z., Bagheri, R., Jahanshahi, R., 2010. Hydrogeochemistry and geothermometry of Changal thermal springs, Zagros region, Iran. Geothermics, 39: 242–249.
Mohammadi, Z., Sahraei Parizi, H., 2013. Hydrogeochemistry and geothermometry of the Jowshan thermal springs, Central Iran. Geochemistry International, 51(12): 994–1004.
Morales–Arredondo, J.I., Esteller–Alberich, M.V., Armienta–Hernández, M.A., Martínez–Florentino, T.A.K., 2018. Characterizing the hydrogeochemistry of two low–temperature thermal systems in Central Mexico. Journal of Geochemical Exploration, 185: 93–104.
Naderi, M., Jahanshahi, R., Dehbandi, Reza., 2020. Two distinct mechanisms of fluoride enrichment and associated health risk in springs' water near an inactive volcano, southeast Iran. Ecotoxicology and Environmental Safety, 195: 110503.
Navarro, J.Á.S., López, P.C., Perez–Garcia, A., 2004. Evaluation of geothermal flow at the springs in Aragón (Spain), and its relation to geologic structure. Hydrogeology Journal, 12: 601–609.
Nieva, D., Nieva, R., 1987. Developments in geothermal energy in Mexico–Part Twelve. A cationic geothermometer for prospecting of geothermal resources. Heat Recovery Systems & CHP, 7(3): 243–258.
Ohmoto, H., 1986. Stable isotope geochemistry of ore deposits. Rev Mineral, 16, 491–560.
Pang, J., Pang, Z., Lv, M., Tian, J., Kong, Y., 2018. Geochemical and isotopic characteristics of fluids in the Niutuozhen geothermal field, North China. Environmental Earth Sciences, 77: 12.
Parisi, S., Paternoster, M., Kohfahl, C., Pekdeger, A., Meyer, H., Hubberten, H.W., Spilotro, G., Mongelli, G., 2011. Groundwater recharge areas of a volcanic aquifer system inferred from hydraulic, hydrogeochemical and stable isotope data: Mount Vulture, southern Italy. Hydrogeology Journal, 19: 133–153.
Parkhurst, D.L., Appelo, C.A.J., 1999. User's guide to PHREEQC (version 2): a computer program for speciation, batch reaction, one–dimensional transport and inverse geochemical calculations. Water Resources Investigations, report 95–4259. US Geological Survey, Denver, Colorado.
Raghimi, M., Yakhkeshi, M.E., 2002. The origin of thermal water of Ziarat, Gorgan by hydrochemistry and isotopic studies. journal of agricultural sciences and natural resources, 9(3): 29–40. (in Persian, with abstract in English).
Rezaei, A., Javadi, H., Rezaeian, M., Barani, S., 2018. Heating mechanism of the Abgarm–Avaj geothermal system observed with hydrochemistry, geothermometry, and stable isotopes of thermal spring waters, Iran. Environmental Earth Sciences, 77(18): 635. https://link.springer.com/article/10.1007/s12665–018–7828–1.
Rezaei, A., Rezaeian, M., Porkhial, S., 2019. The hydrogeochemistry and geothermometry of the thermal waters in the Mouil Graben, Sabalan volcano, NW Iran. Geothermics, 78: 9–27.
Rittenhouse, G., 1967. Bromine in oil–field waters and its use in determining possibilities of origin of these waters. AAPG Bull, 51(15): 2430–2440.
Rybach, L., Muffler, L.J.P., 1981. Geothermal Systems: Principles and Case Histories. John Wiley & Sons Ltd, The Pitman Press, Bath, Avon, UK, 359.
Saadat, S., Stern, C.R., 2011. Petrochemistry and genesis of olivine basalts from small monogenetic parasitic cones of Bazman stratovolcano, Makran arc, southeastern Iran. Lithos, 125: 607–619.
Sharifi, R., Moore, F., Mohammadi, Z., Keshavarzi, B., 2016. Estimation of deepwater temperature and hydrogeochemistry of springs in the Takab geothermal field, West Azerbaijan, Iran. Environmental Monitoring and Assessment, 188: 75.
Sutherland, R., Townend, J., Toy, V., Upton, P., Coussens, J., Allen, M., Baratin, L. M., Barth, N., Becroft, L., Boese, C., Boles, A., Boulton, C., Broderick, N.G.R., Janku–Capova, L., Carpenter, B.M., Célérier, B., Chamberlain, C., Cooper, A., Coutts, A., Cox, S., Craw, L., Doan, M.L., Eccles, J., Faulkner, D., Grieve, J., Grochowski, J., Gulley, A., Hartog,

A., Howarth, J., Jacobs, K., Jeppson, T., Kato, N., Keys, S., Kirilova, M., Kometani, Y., Langridge, R., Lin, W., Little, T., Lukacs, A., Mallyon, D., Mariani, E., Massiot, C., Mathewson, L., Melosh, B., Menzies, C., Moore, J., Morales, L., Morgan, C., Mori, H., Niemeijer, A., Nishikawa, O., Prior, D., Sauer, K., Savage, M., Schleicher, A., Schmitt, D.R., Shigematsu, N., Taylor–Offord, S., Teagle, D., Tobin, H., Valdez, R., Weaver, K., Wiersberg, T., Williams, J., Woodman, N., Zimmer, M., 2017. Extreme hydrothermal conditions at an active plate–bounding fault. Nature, 1546 (7656): 137–140.

Truesdell, A.H., Fournier, R.O., 1977. Procedure for estimating the temperature of a hot–water component in a mixed water using a plot of dissolved silica vs. enthalpy. US Geol Surv J Res 5, 49–52.

Yazdi, M., Taheri, M., Navi, P., 2015. Environmental geochemistry and sources of natural arsenic in the Kharaqan hot springs, Qazvin, Iran. Environmental Earth Sciences, 73(9): 5395–5404.